Top Catal (2012) 55:391–401
DOI 10.1007/s11244-012-9796-0

ORIGINAL PAPER

Theoretical Investigation of Hydrogen Adsorption and Dissociation on Iron and Iron Carbide Surfaces Using the ReaxFF Reactive Force Field Method

Chenyu Zou · Adri C. T. van Duin · Dan C. Sorescu

Published online: 20 April 2012

Abstract We have developed a ReaxFF reactive force field to describe hydrogen adsorption and dissociation on iron and iron carbide surfaces relevant for simulation of Fischer–Tropsch (FT) synthesis on iron catalysts. This force field enables large system (>>1000 atoms) simulations of hydrogen related reactions with iron. The ReaxFF force field parameters are trained against a substantial amount of structural and energetic data including the equations of state and heats of formation of iron and iron carbide related materials, as well as hydrogen interaction with iron surfaces and different phases of bulk iron. We have validated the accuracy and applicability of ReaxFF force field by carrying out molecular dynamics simulations of hydrogen adsorption, dissociation and recombination on iron and iron carbide surfaces. The barriers and reaction energies for molecular dissociation on these two types of surfaces have been compared and the effect of subsurface carbon on hydrogen interaction with iron surface is evaluated. We found that existence of carbon atoms at subsurface iron sites tends to increase the hydrogen dissociation energy barrier on the surface, and also makes the corresponding hydrogen dissociative state relatively more stable compared to that on bare iron. These properties of iron carbide will affect the dissociation rate of H_2 and will retain more surface hydride species, thus influencing the dynamics of the FT synthesis process.

C. Zou · A. C. T. van Duin (✉)
Department of Mechanical and Nuclear Engineering, Pennsylvania State University, University Park, PA 16802, USA
e-mail: acv13@psu.edu

D. C. Sorescu
National Energy Technology Laboratory, U.S. Department of Energy, Pittsburgh, PA 15236, USA

Keywords Fischer–Tropsch synthesis · Hydrogen dissociation and reformation · Iron and iron carbide · ReaxFF

1 Introduction

Fischer–Tropsch (FT) synthesis consists of a series of chemical reactions that transform a mixture of hydrogen and carbon monoxide (often called syngas) to form liquid hydrocarbons. In typical industrial applications, syngas can be produced from water and coal. Though its practical applicability strongly depends on the price of crude oil [1], FT synthesis does have its advantages in producing clean fuels and thus offers an important alternative for fuel production to crude oil. Metals such as iron, cobalt, and nickel are usually used as catalysts for these reactions.

Essential initial steps of the synthesis include chemisorption and dissociation of the syngas on the surface of the catalyst. In the case of iron, the reaction mechanism is further complicated since the metal tends to transform to a carbide upon CO chemisorption and decomposition, with corresponding structural and phase changes, leading, for example, to a magnetite core surrounded by an iron carbide shell [2]. Thus, it is important to analyze the syngas dissociation properties on both iron and iron carbide structures.

Several experimental studies [3–7] have already reported the analysis of the absorption and dissociation properties of H_2 species on the low index iron surfaces. In addition, atomistic scale simulations of H_2 interaction with a variety of iron surfaces and bulk iron phases have been performed using either semi empirical methods [8] or first principles calculations [9–13]. These theoretical studies addressed various properties of the hydrogen-iron interaction including: site preference, surface and subsurface adsorption

energies, surface to subsurface and further to bulk diffusion. Among various quantum mechanics (QM) based methods, density functional theory (DFT) is widely used to study catalytic systems. A recent research example of how DFT were used to explore a related system can be found in Ref. [14]. Among the major limitations of such QM methods which handle explicitly the electron–electron interactions is the size of the systems that can be described efficiently, generally restricted to hundreds of atoms, and for duration not exceeding several femtoseconds. In the FT related studies, DFT methods have been used to study the properties of metal related surfaces [15] and bulk phases [16], the chemisorptions properties of small molecular systems such as CO, H_2, or C_xH_y, or the interactions of the atomic C/H/O species with catalyst surfaces or bulk phases [11–13, 15, 17–23]. Description of practical reactions involving diverse problems such as chemical kinetics, reaction dynamics, and interactions of various complex materials require, however, the analysis of system size and time scale well beyond the current limits of typical QM calculations.

To close the gap between QM calculations and experiments, traditional molecular dynamics (MD) simulations can be employed to treat larger systems and for longer times. These MD methods use specialized force fields to describe the interatomic interactions. A classic example for such a general force field is shown in Ref. [24]. However, many of these traditional force fields employ simple harmonic type of bond description, and consequently are not capable to describe either bond formation or bond cleavage correctly.

One of the approaches to describe reactions in MD simulations is to develop force fields which implicitly embed the effects of electron–electron interactions. Such reactive force fields utilize chemical concepts such as bond order and electronegativity and are able to correctly describe chemical reactions. However, many of these reactive force fields are designed for specific systems and generally lack transferability beyond the systems for which were originally developed.

In this study, we report the development and application of a highly transferable reactive force field for C/H/Fe system. ReaxFF potential has been developed for systems related to FT synthesis including hydrocarbons [25], metal and metal oxides [26, 27], metal hydrides [28, 29], and interactions among these species [30, 31]. These studies indicate the applicability of ReaxFF concept to catalytic systems and the transferability of the force field among these systems of different species. Recently, Ashwin et al. [32] developed an interatomic potential for a related H/Fe system, which provided a description of bulk Fe-metal and metal hydride phases. In addition to the structures described by the Ashwin-potential, ReaxFF is capable of performing MD simulations on reactions between gas phase molecules interacting with solid surfaces. Reference [33] shows a recent ReaxFF investigation of a FT synthesis type of system, where nickel is used to catalyze the decomposition of gas phase C_xH_y species. We also reported the O/H/Fe interactions in Ref. [34]. Here we have combined this O/H/Fe description with previous C/H data, and extend these parameters to describe iron carbide species. ReaxFF parameters are trained against several sets of quantum data including the iron metal and carbide equations of state, the hydrogen binding energies on iron bcc (100) and (110) surfaces at different surface sites and for different surface coverage, and the hydrogen diffusion path in the bulk phase metal. These ReaxFF parameters developed were then used to analyze the dissociation pathway of a single H_2 molecule on pure iron bcc (100) surface and on a surface with a subsurface carbon atom, respectively. The force field parameters are further tested through MD simulations of hydrogen dissociation on iron and iron carbide clusters at low temperature around a typical FT-synthesis temperature range (470 $\sim$ 620 K), followed by MD-simulations at elevated temperatures to observe possible hydrogen recombination and desorption from the surface. The rates of H_2 dissociation and reformation on the pure metal and carbide surfaces are also compared.

The rest of this paper is organized as follows: in Sect. II a general description of DFT and ReaxFF computational methods used is provided; in Sect. III the force field parameters training results are described, followed by MD simulation of hydrogen dissociation and reformation. Finally in Sect. IV, the main conclusions are summarized and directions for future work are presented.

2 Computational Methods

2.1 QM Method

The ReaxFF reactive force field parameters are trained against results from first principles calculations based on spin-polarized DFT. In DFT calculations, both the projector-augmented-wave (PAW) method [35] and ultrasoft pseudopotentials (USPP) method [36] were used to describe the electron–ion interaction while the generalized gradient approximation (GGA) was used for the treatment of exchange and correlation. The equation of state of bulk phase iron was fitted to Murnaghan's equation of state [37]. Diffusion of H_2 on both (100) and (110) surface or from these surfaces to subsurface and farther to bulk were calculated using the climbing-image nudged elastic band (CI-NEB) method [38]. This method allows locating both the minimum energy pathways (MEP) among various local minima as well as the corresponding transition state. DFT data from Refs. [20], [16] and [39] related to the bulk phase iron, Fe_5C_2 surface energies and the Fe_3C equation of state were used to parameterized the ReaxFF force field.

2.2 ReaxFF Reactive Force Field [25]

ReaxFF is an empirical force field that employs bond-length/bond-order and bond-order/bond-energy relationships to get smooth transition between bonded and non-bonded systems. Bond orders are calculated from interatomic bond lengths using the following equation:

$$BO_{ij} = BO_{ij}^{\sigma} + BO_{ij}^{\pi} + BO_{ij}^{\pi\pi} = \exp[p_{bo1}(\frac{r_{ij}}{r_0^{\sigma}})^{p_{bo2}}] + \exp[p_{bo3}(\frac{r_{ij}}{r_0^{\pi}})^{p_{bo4}}] + \exp[p_{bo5}(\frac{r_{ij}}{r_0^{\pi\pi}})^{p_{bo6}}]$$

.

The bond orders are updated every iteration during an MD run and the system potential energy is bond order dependent. ReaxFF has the advantage over early time reactive force fields in that it includes non-bonded interactions, including van der Waals and Coulomb terms, which are calculated between each pair of atoms. These features make this method transferable among covalent, ionic and metallic systems. ReaxFF uses an electronegativity equilibration method (EEM) [40] with shielding [41] to calculate the charge distribution. Force field parameters are trained against QM data using a single-parameter search optimization method [42]. Beside the structural and energetic data mentioned before the training set also include the activation energies and the heats of reaction for various chemical reactions or diffusion processes, thus allowing ReaxFF to capture the kinetics of chemical reactions.

3 Results and Discussion

3.1 Force Field Parameter Development

We began to train the force field parameters with the previously published ReaxFF description of iron-oxyhydroxide [34] and hydrocarbons [25]. To capture the hydrogen adsorption and dissociation on iron and iron carbide surface, the force field parameters were optimized against an extensive set of structures describing iron–iron, iron-hydrogen and iron-carbon bonding characters. These structures include the iron bcc and fcc bulk phase equation of state (EOS), the Fe_3C cementite EOS as well as several structures describing hydrogen binding with iron and iron carbide surfaces and bulk phases. Sets of selected optimized parameters are presented in Tables 1, 2, 3, 4.

3.2 Fe/Fe Interaction

In order to correctly describe the iron bulk and the corresponding surface energies in different chemical configurations, we trained the iron–iron interaction to reproduce not only the iron crystal at ambient conditions, but also the bulk phase under compression and expansion conditions. In our current force field parameters, the energy of the optimized bcc bulk phase iron is 3.17 kcal/mol lower than the fcc bulk phase iron, compared with a 3.64 kcal/mol from DFT data. The bulk lattice constant predicted by ReaxFF is 2.84 Å, compared with 2.86 Å [36] and 2.83 Å [35] from DFT data, using USPP and PAW respectively. Experimental value shows a value of 2.86 Å [43]. Figure 1 compares the relative energies of bulk bcc iron upon

Table 3 ReaxFF fit for C/H/Fe selected off diagonal bond parameters (D_{ij} in kcal/mol, R_{vdW}, r_o^{σ} and r_o^{π} in Å, all the other parameters are unitless)

	D_{ij}	R_{vdW}	α	r_o^{σ}
C–H	0.1239	1.4004	9.8467	1.1210
C–Fe	0.3219	1.4560	10.9553	1.4329
H–Fe	0.0208	1.8797	11.0601	1.3942

Table 1 ReaxFF fit for Fe parameters (r_o^{σ} and r_{vdW} in Å; $D_{ij}$and D_e^{σ} in kcal/mol; all the others are unitless)

Atom	r_o^{σ}	r_{vdW}	D_{ij}	α	γ_w
Fe	1.9029	2.099	0.1181	10.8548	2.6084
Bond	D_e^{σ}	$p_{be,1}$	$p_{ovun,1}$	$p_{be,2}$	$p_{bo,1}$	$p_{bo,2}$
Fe–Fe	41.4611	0.2931	0.2682	0.6294	-0.0512	6.8013

For a definition of the parameters, see reference [25]

Table 2 ReaxFF fit for C/H/Fe bond parameters (D_e^{σ} and D_e^{π} in kcal/mol, all the other parameters are unitless)

Bond	D_e^{σ}	$p_{be,1}$	$p_{ovun,1}$	$p_{be,2}$	$p_{bo,1}$	$p_{bo,2}$	$p_{bo,3}$	$p_{bo,4}$
C–Fe	103.2582	0.8660	0.01	0.9651	−0.1399	4.3334	−0.35	15
H–Fe	77.3903	0.4011	0.1228	0.6165	−0.1658	5.2955		

For a definition of the parameters, see reference [25]

Table 4 ReaxFF fit for C/H/Fe selected angle parameters (Θ_0 in deg, all the other parameters are unitless)

	Θ_0	k_a	k_b	$p_{val,2}$	$p_{val,3}$
C–Fe–C	45.0534	43.7115	0.1742	1.4685	1.8494
C–C–Fe	74.8790	30.0000	2.0000	2.0334	1.0928
C–Fe–Fe	63.3653	1.8828	8.0000	2.7499	1.0000
Fe–C–Fe	26.2341	50.0000	0.9167	0.2434	1.2411
H–C–Fe	2.0180	37.8528	0.9638	0.1000	1.2681
H–Fe–H	24.6837	3.3477	1.6305	1.0588	1.7646
H–H–Fe	0.0000	0.0100	1.0097	2.8060	3.5303
Fe–H–Fe	0.0000	11.3293	5.6628	0.1500	1.2948
H–Fe–Fe	32.7903	3.9308	1.3508	1.5730	2.4170
C–Fe–H	44.1263	0.1498	0.3274	0.1020	2.0703
C–H–Fe	0.0000	5.0000	2.0000	1.0000	1.5000

compression and expansion as determined from DFT [20] and ReaxFF. The force field parameters were trained against the QM derived equations of state for ferromagnetic (FM) bcc and fcc bulk phases [20] and the antiferromagnetic double-layer (AFMD) phase of iron. The DFT-results for fcc-FM show a double well, related to a low-spin transition to a high-spin state, as described in detail by Jiang and Carter [20]. Since ReaxFF does not include a magnetic term, we decided to fit against the lowest-energy magnetic bcc and fcc phases at all volumes. Figure 1 shows that our current parameters successfully reproduce the variation of the energies of bcc and fcc bulk phase around the equilibrium region and for small external stresses. In high stress situations, there is a larger difference between QM and ReaxFF but they are acceptable as long as ReaxFF can recognize these structures as energetic undesirable and avoid them in a typical chemical environment. This also indicates that our current force field parameters may be less accurate to predict the material properties under an extreme mechanical environment with high stress.

The ReaxFF bcc (100) and (110) surface energies are 14.5 and 9.96 kcal/mol respectively, which compare well to the values of 14.38 and 9.78 kcal/mol obtained from DFT calculations [44].

3.3 C/Fe Interactions

As mentioned previously, during FT synthesis the iron surface is transformed slowly to a carbide surface as a result of carbon monoxide adsorption and dissociation on the surface and carbon atom migrating to the subsurface. At equilibrium the catalyst is transformed to an iron carbide phase while the resulting oxygen is eliminated as water. Thus, it is important to include in the training set structures and energetic data for bulk iron carbide and different corresponding surfaces.

The heat of formation of Fe_3C (cementite) predicted by ReaxFF is 5.94 kcal/mol, compared to 4.14 kcal/mol from QM prediction [45] and 4.37 kcal/mol from experimental measurements [46]. Figure 2 shows the equations of state for cementite predicted by ReaxFF and DFT data[16], respectively. Figure 3 shows a comparison of various low Miller index Fe_5C_2 surface energies between ReaxFF and DFT data [39]. These results indicate that we have good agreement describing iron carbide species between ReaxFF and QM methods.

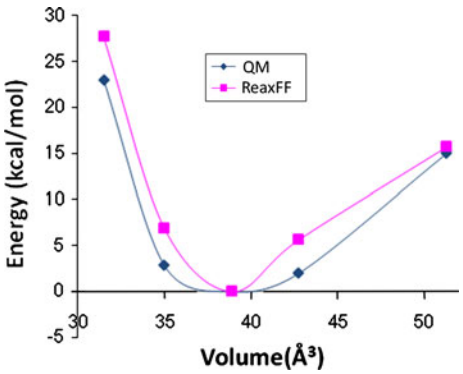

Fig. 2 ReaxFF fit for the equation of state for Fe_3C cementite

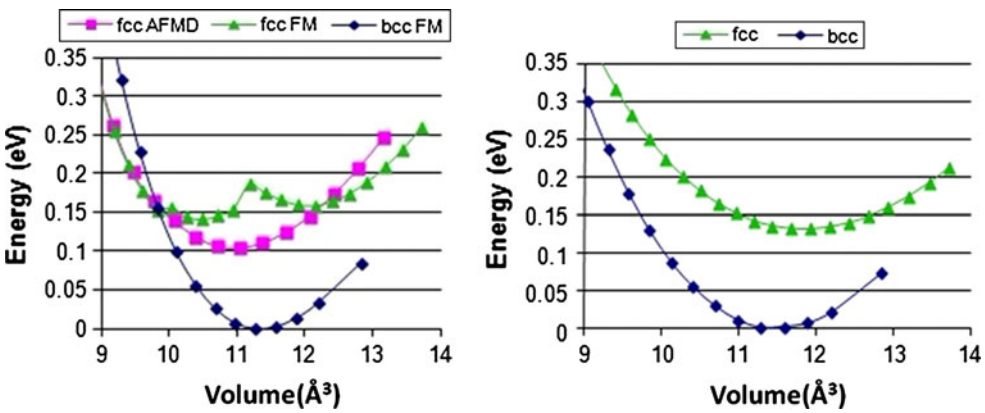

Fig. 1 Comparison of the ReaxFF fit (*right panel*) of the EOS for bcc and fcc bulk phases of iron with the corresponding QM data (*left panel*) for the bcc (FM), fcc (FM) and fcc(AFMD) as obtained in Ref. [20]

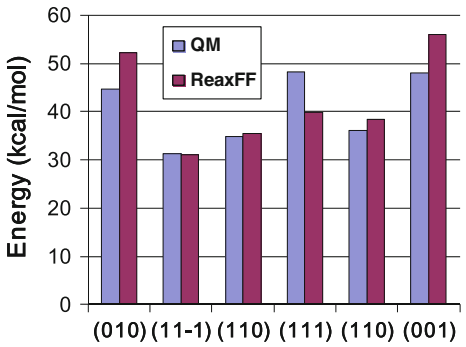

Fig. 3 Comparison of Fe_5C_2 surface energies for several low Miller indices obtained using QM and ReaxFF methods

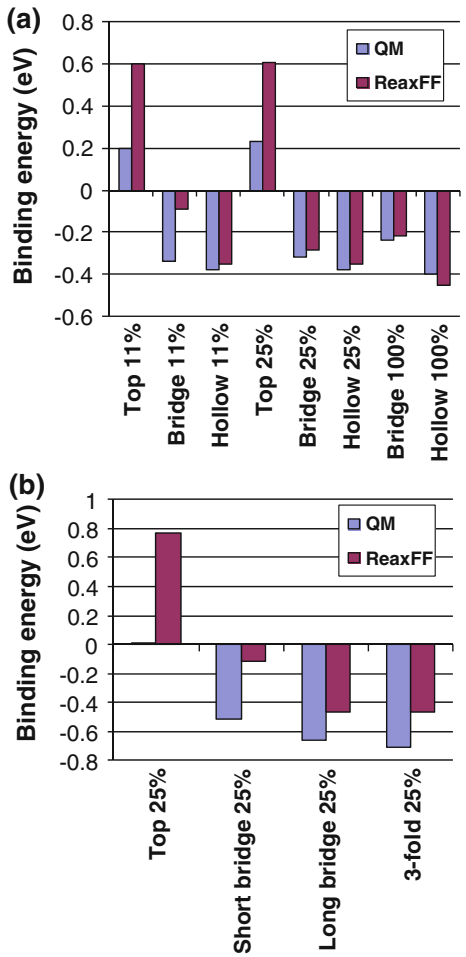

Fig. 4 ReaxFF fit for binding energies of H atom at various sites on (**a**) Fe (100) and (**b**) Fe (110) surfaces

3.4 H/Fe Interactions

Figure 4 shows the hydrogen binding energies at different sites of Fe bcc (100) and Fe (110) surfaces and for three different surface coverages. We observe that ReaxFF provides a good agreement with DFT data [12] particularly for the case of binding at the most stable bridge and hollow sites but underestimates the adsorption energies at the top sites on both (100) and (110) surfaces. This limitation is however not problematic as the adsorption at the top sites on both surfaces is not stable and the adsorbed H_2 molecule at such sites will quickly move to the nearby bridge or hollow sites which provide stable local minima.

To ensure our force field provides an accurate description of the C/H/Fe system, structures describing the hydrogen interacting with bulk phase metal were also included in our fitting analysis and the corresponding results are indicated in Fig. 5. Panel 5A indicates the binding energies of hydrogen absorbed at Fe bulk vacancy sites, while panels 5B-5D show three hydrogen diffusion pathways. The iron hydride heat of formation predicted by ReaxFF is 1.73 kcal/mol, which is in good agreement with the QM value of 1.888 kcal/mol [47].

3.5 Hydrogen Dissociation Pathways

As indicated above, hydrogen dissociation on iron and iron carbide surface is one of the primary initial steps of FT synthesis. As such, we have to make sure that our force field captures the corresponding H_2 chemisorption and dissociation steps correctly. Figure 6 shows one of the hydrogen dissociation pathways on iron bcc (100) surface as predicted by ReaxFF. A H_2 molecule was initially placed above the iron surface in between two-forth fold hollow sites and oriented perpendicular to the iron–iron bond. With a bond restraining technique, we gradually force the hydrogen molecule to get dissociatively chemisorbed to the two hollow sites. The energy barrier found in this case is 4.06 kcal/mol and the reaction energy is −16.99 kcal/mol.

A similar dissociation pathway was found using DFT-method [13] with an energy barrier of 3.87 kcal/mol and a reaction energy of about −15 kcal/mol. Note that this dissociation pathway was not included in the training process, and the reasonable agreement found between ReaxFF and QM method indicates the versatility of our ReaxFF parameters.

Another dissociation pathway we analyzed is shown in Fig. 7. In this case, a hydrogen molecule was initially placed above a hollow site on iron bcc (100) surface and was dissociatively chemisorbed to two bridge sites located on opposite sides relative to the original hollow site. The corresponding energy barrier is 4.4 kcal/mol and the reaction energy is about −9 kcal/mol. Considering that the hollow site adsorption is energetically more stable by 3.7 kcal/mol than a bridge site [10], this reaction energy is acceptable.

These results are in good agreement with previous experimental reports [3], which indicate that

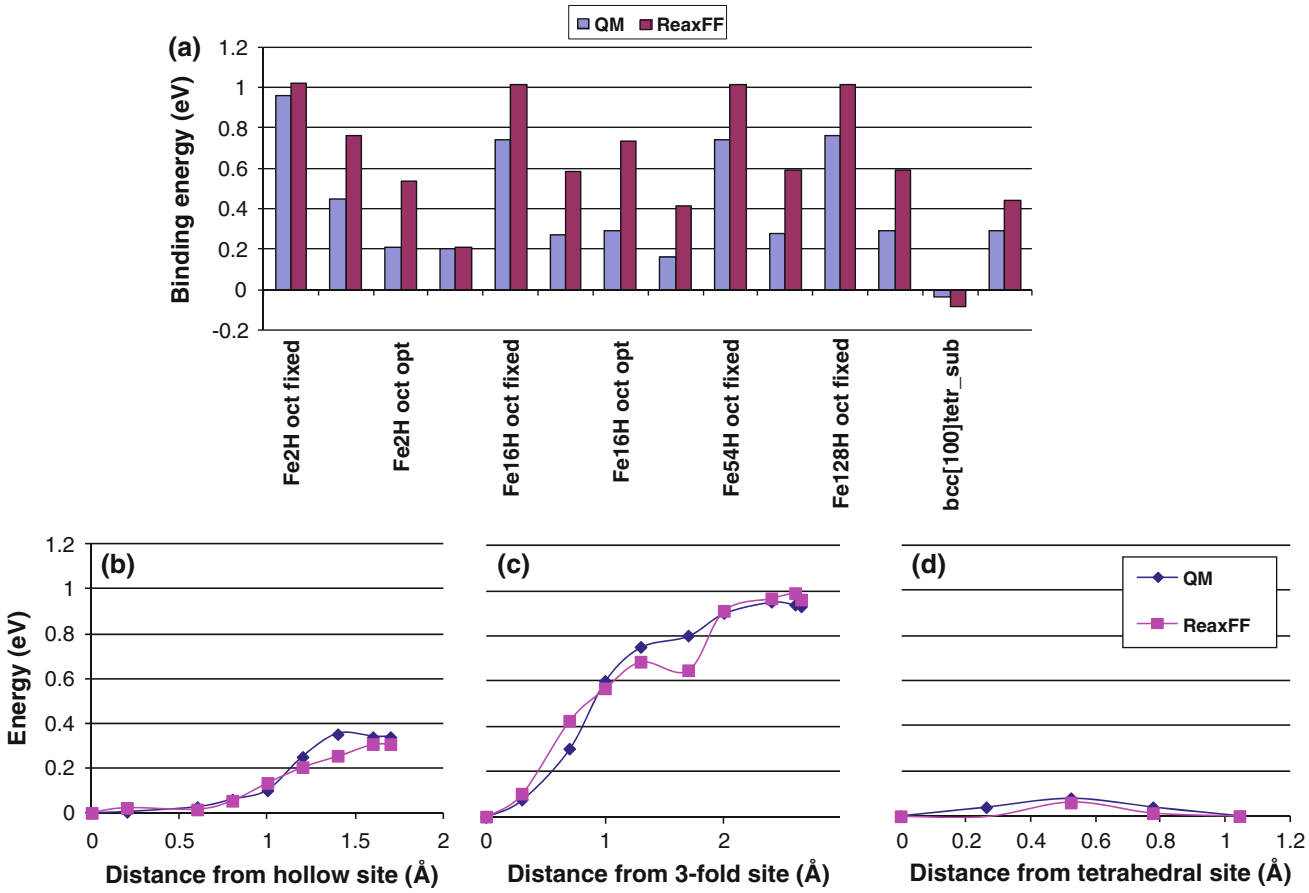

Fig. 5 ReaxFF fit for **a** Binding energies of H atom to different vacancies in bulk phase iron, **b** H diffusion pathway from a (100) surface hollow site to a subsurface tetrahedral site, **c** H diffusion pathway from a (110) surface three-fold site to subsurface tetrahedral site, **d** H diffusion pathway among two nearby subsurface tetrahedral sites in a FeH-bulk phase

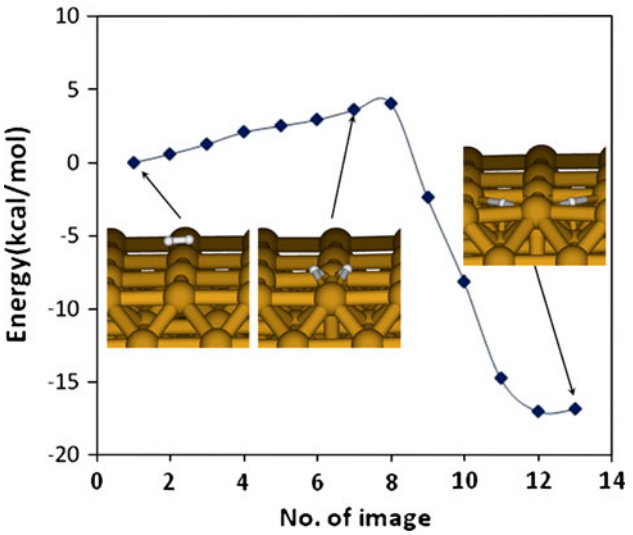

Fig. 6 Hydrogen dissociation pathway on a Fe(100) surface starting from a two-fold site above the surface and ending to two neighbor four-fold hollow sites

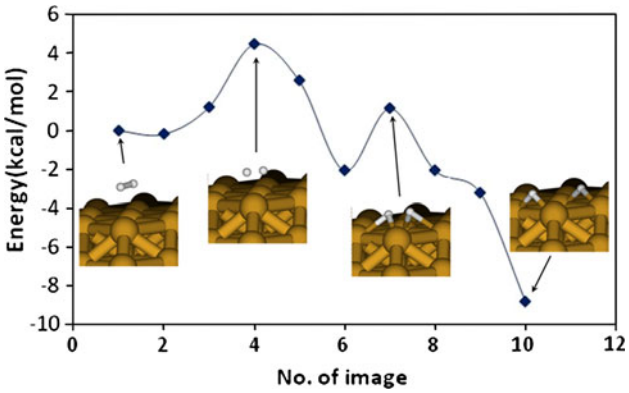

Fig. 7 Hydrogen (indicated by *white* dots) dissociation pathway on Fe(100) surface (indicated by *yellow* dots) starting from a state above the hollow site and ending to two dissociated H atoms adsorbed at two opposite bridge sites

chemisorptions of hydrogen can take place on iron surface very rapidly indicating the existence of small energy barriers.

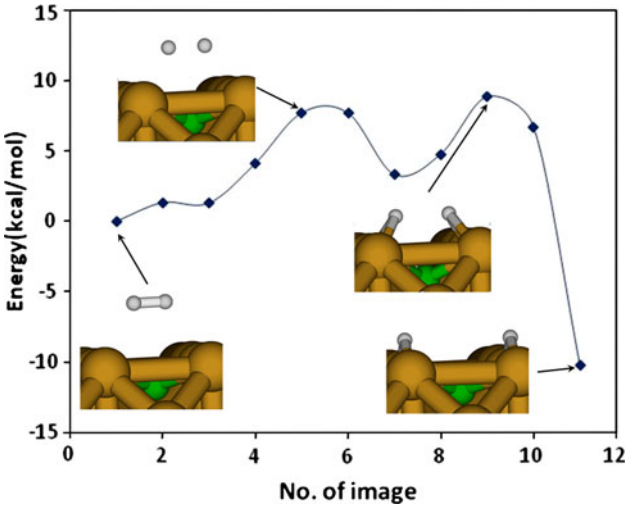

Fig. 8 Hydrogen dissociation pathway on Fe (100) to two bridge sites facing each other in the case of the subsurface carbon atom (*green*)

We also studied the hydrogen dissociation on iron in the case of a surface with an adsorbed subsurface carbon atom. Figure 8 shows such a dissociation pathway. In the case of the surface with a subsurface adsorbed carbon atom the energy barrier increase to 9.5 kcal/mol. This value is about 5 kcal/mol higher than that obtained for the case of bare Fe surface. The corresponding reaction energy is −10.5 kcal/mol, slightly higher compared with the same dissociative configuration on pure iron surface (−9 kcal/mol), indicating that this hydrogen dissociated state is more stable on the surface with subsurface C than on the bare Fe surface. Exactly why the existence of a subsurface carbon atom makes this reaction more exothermic is not straightforward; it could be related to the fact that carbon is more electronegative than iron, which makes the iron carbide more reactive towards electropositive elements like hydrogen.

3.6 Application of the Force Field in MD Simulations

3.6.1 MD Simulations of Hydrogen Dissociation

To provide an application of the aforementioned ReaxFF H/C/Fe description, we set up two systems as indicated in Fig. 9.

System I is an iron cluster of 432 atoms with its (100) surface exposed to gas phase hydrogen. System II is a cementite (Fe_3C) cluster of 512 atoms having also the (100) surface exposed to hydrogen. After energy minimization, both systems were subject to molecular dynamics simulation in the NVT ensemble for 250 ps and at different temperatures. The temperature was controlled using a Berendsen thermostat with a damping constant of 100 fs.

Figure 10 shows the iron hydride cluster at 500, 600 and 750 K after 250 ps as indicated in panels A, B, and C respectively. Since 750 K is higher than a typical FT synthesis temperature range (470 ∼ 620 K), we performed simulations at this temperature for force field validation purposes. Compared to 500 K case, where the surface and the cluster maintained the original shape, we begin to

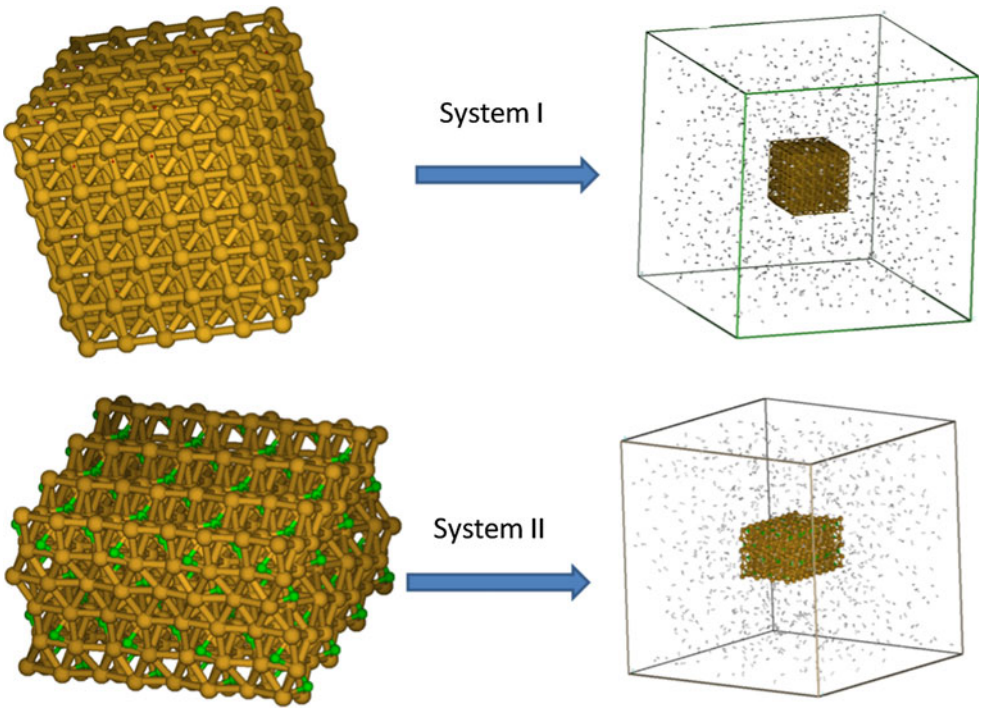

Fig. 9 MD simulation setups for two cluster systems of (I) iron and (II) cementite

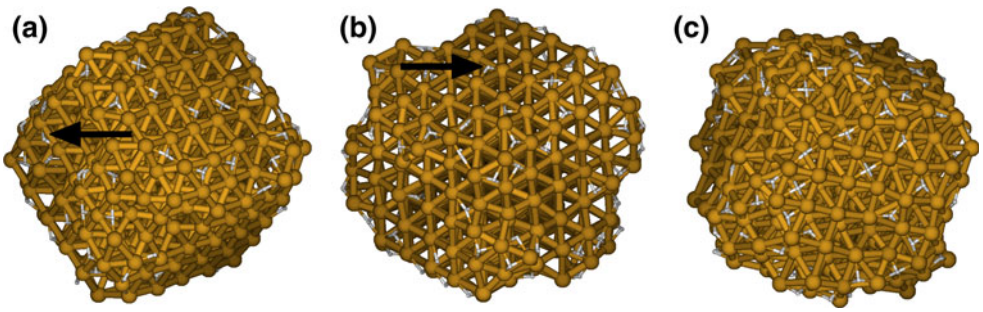

Fig. 10 Iron hydride cluster after 250 ps and H_2 exposure at: **a**, 500 K; **b**, 600 K; **c**, 750 K. *Yellow* dots: Fe; *White* dots: hydrogen

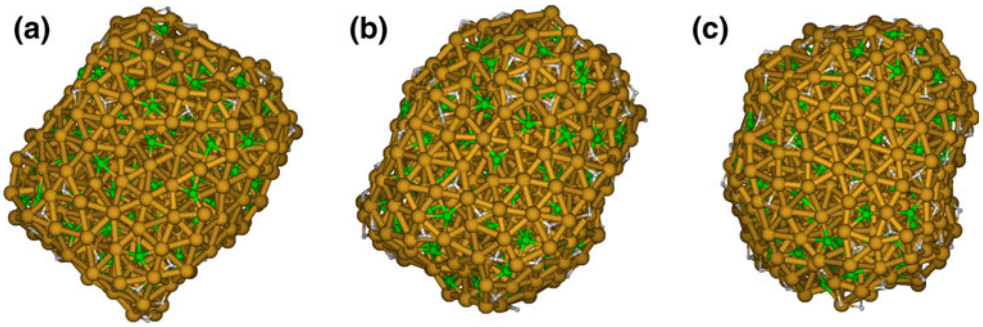

Fig. 11 Iron carbide hydride cluster after 250 ps and hydrogen exposure at: **a**, 500 K; **b**, 600 K; **c**, 750 K. *Yellow* dots: Fe; *White* dots: hydrogen; *Green* dots: carbon

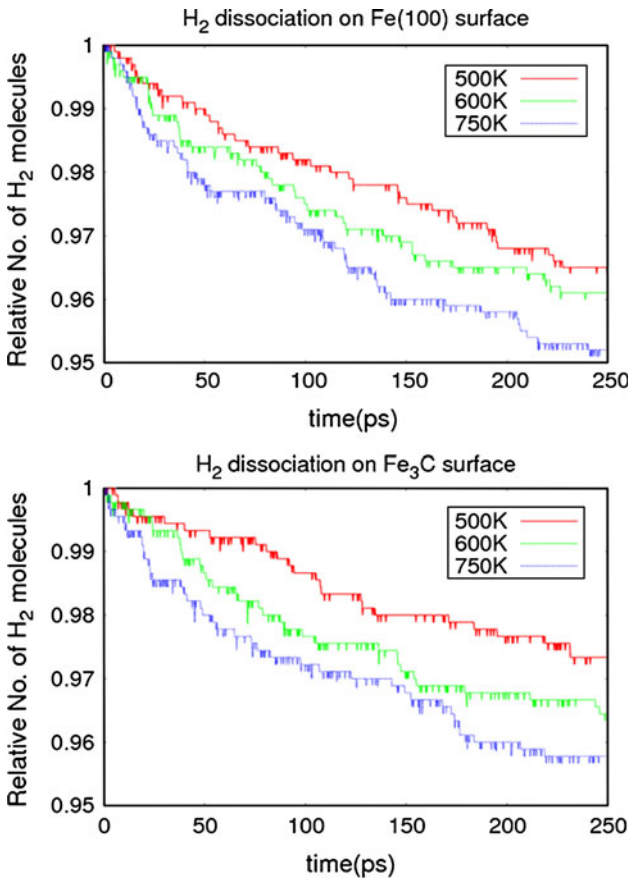

Fig. 12 H_2 gas phase concentration profiles as a function of time, temperature, and cluster composition

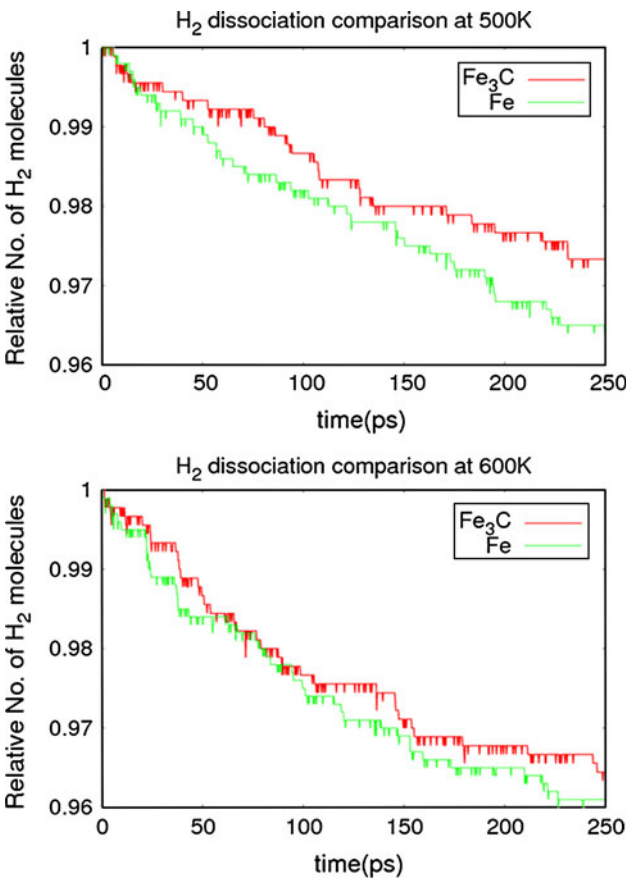

Fig. 13 Comparison of H_2 dissociation kinetics for Fe- and Fe-carbide clusters at 500 and 600 K

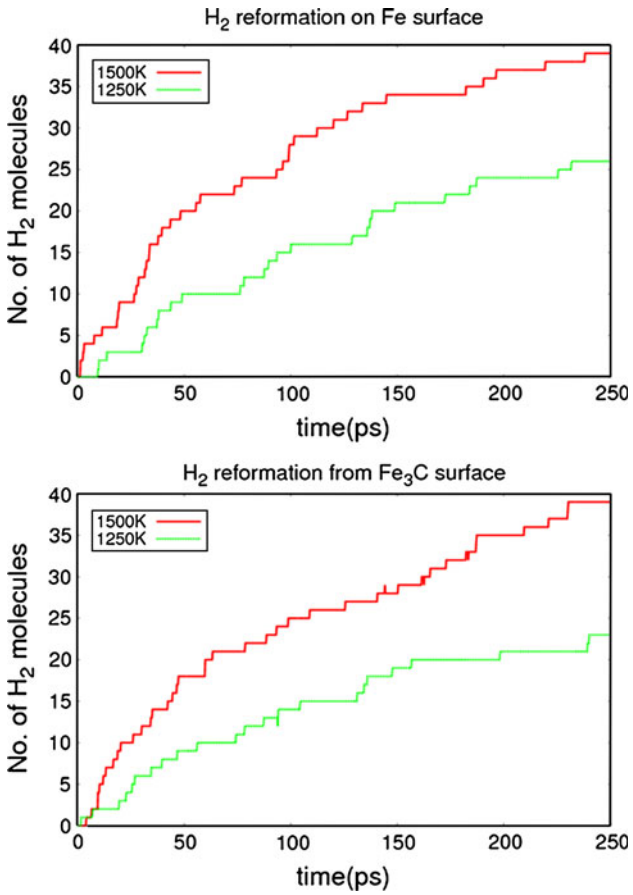

Fig. 14 H_2 reformation kinetics for the Fe- and Fe-carbide particle at T = 1250 and 1500 K

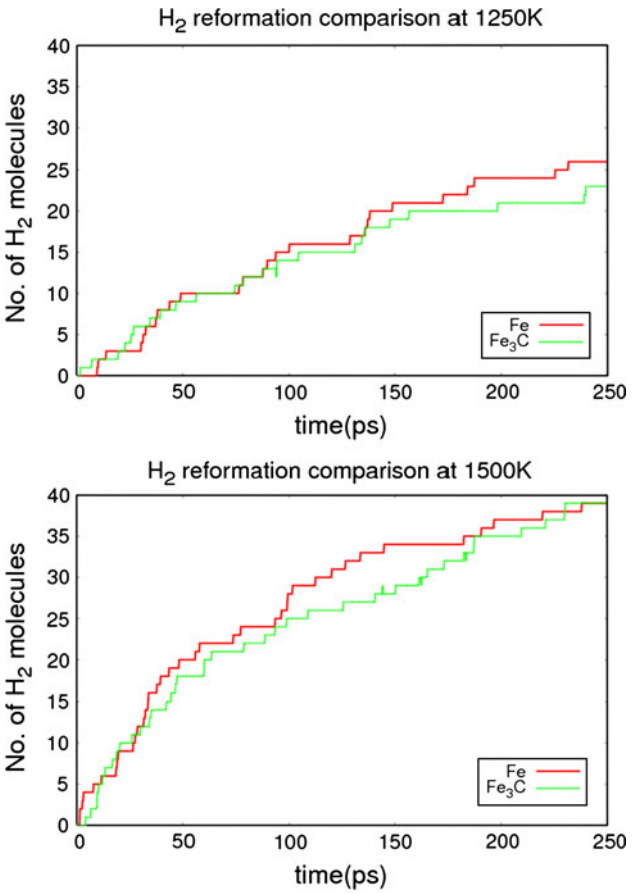

Fig. 15 Comparison of H_2 reformation kinetics for a Fe- and Fe-carbide particle at T = 1250 and 1500 K

observe cluster deformation at 600 and 750 K. The active sites including the bridge and hollow sites for hydrogen dissociation are still recognizable. This figure also shows that most of the gas phase hydrogen molecules dissociated at the four-fold hollow sites, indicating that these sites are more stable than the top and bridge sites. We also observed dissociated hydrogen atoms adsorbed at bridge sites (as pointed by black arrow), in agreement with previous QM results [13] which indicate that bridge sites are stable for atomic hydrogen.

Figure 11 shows in panels A, B and C the iron carbide hydride cluster at 500, 600, and 750 K after 250 ps, respectively. In this case, we can see that the cluster and the surface are substantially deformed, especially at high temperature (750 K), and the original (100) surface is hardly recognizable. This suggests that cementite clusters with exposed (100) surface are not very stable, particularly at temperatures in excess of 750 K.

Figure 12 shows the variation of the number of gas phase H_2 molecules for the Fe (100) and Fe_3C (100) systems. The number of hydrogen molecules as indicated by the y axis is normalized with respect to the initial amount. ReaxFF clearly predicted an increase in hydrogen dissociation rates as the temperature increases.

More importantly, a comparison of the H_2 dissociation rate between these two clusters (Fig. 13) at the same temperature shows that in a typical high temperature FT synthesis temperature range, the dissociation rate of hydrogen is higher on pure iron cluster than on iron carbide cluster, due to a lower energy barrier given by current force field as discussed earlier in this paper.

3.7 MD Simulations of Hydrogen Desorption at High-Temperature

After finishing the dissociation simulations presented in the previous section, we extract the hydrogenated iron and iron carbide clusters from systems I and II and placed them in vacuum under elevated temperature to observe hydrogen desorption from the surface. The results are shown in Fig. 14.

Note that the simulations were performed at temperatures of 1250 and 1500 K. These are significantly higher than the typical experimental values linked to H_2

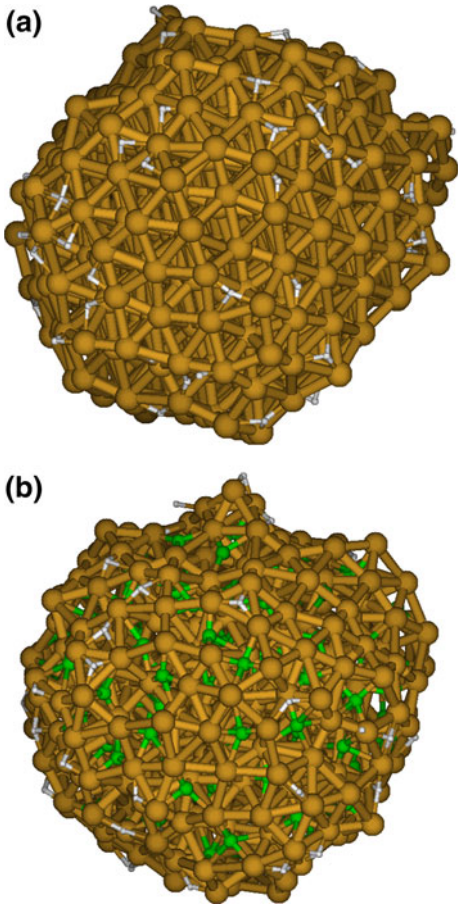

Fig. 16 Final structures of the Fe- (**a**) and Fe-carbide (**b**) particle at the end of the 1500 K ReaxFF simulation

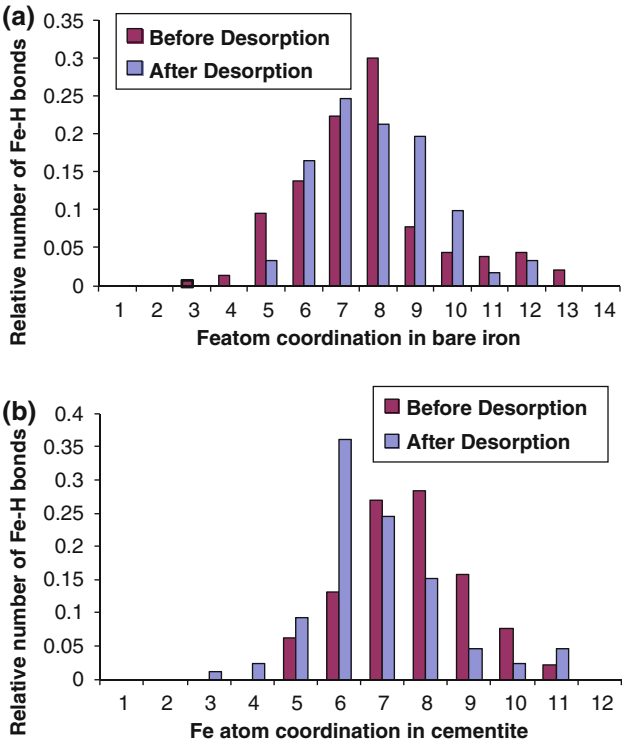

Fig. 17 Fe atom coordination analysis for pure iron (**a**) and cementite cluster (**b**) after hydrogen desorption process at 1500 K

formation, since our simulations cover a relatively short time-duration, so we have to carry out the simulations at high temperature in order to accelerate the process. As noticed previously in Sect. 3.1.4, the single molecule dissociation pathway indicates that the hydrogen dissociation state is more stable on iron carbide compared to pure iron. From Fig. 15, we can see that the hydrogen desorption rate is indeed slightly lower from the hydrogenated iron carbide particle, which agrees with single-molecule observations described in Sect. 3.1.4.

Pictorial views of the iron and iron carbide clusters at the end of the 250 ps simulation of the hydrogen desorption process at 1500 K are shown in panels A and B of Fig. 16. At such high temperature, the original surface is hardly recognizable in both cases, but we observe that the remaining hydrogen tends to diffuse to and bond with the iron atoms at the relatively irregular surface edges. From Fig. 17 panel A we can see that before desorption, the eight-fold coordinated iron atoms possess the maximum portion of the total Fe–H bonds due to the fact that most of the hydrogen dissociates to a four-fold hollow sites. After desorption, the relative number of Fe–H bonds possessed by over coordinated iron atoms (11, 12 and 13 coordinated) decreases. This trend is more obvious in the cementite case as can be seen in Fig. 17 panel B, where the high coordinated iron atoms (7, 8, 9 and 10 coordinated) possess less Fe–H bonds after desorption than before. This observation indicates that the hydrogen atoms remaining on the surface tend to diffuse toward the low-coordinated iron atom. This may relate to the relative high binding energy of hydrogen to these atoms. This phenomena increases the stability for the under coordinated sites on the catalysts surface.

4 Conclusions

We report the development of a set of ReaxFF parameters describing interactions of C/H/Fe systems. These parameters were fitted against an extensive QM and experimental data including equation of states, hydrogen binding energies on low index iron surfaces, and hydrogen interaction with bulk phase metal. Overall, our results show a good agreement with both DFT and experimental data. Based on these parameters, we have examined the hydrogen dissociation and desorption on iron and iron carbide surface. Comparison between these two cases indicates that: the hydrogen dissociation energy barrier is higher in the iron carbide case than in the pure iron case, and the corresponding dissociated state is more stable on the carbide. We applied this ReaxFF Fe/C/H description

in a series of low and high temperature molecular dynamics simulations. In these MD-simulations we observed hydrogen dissociation at low temperatures ($T < 750$ K) and H_2 recombination and desorption from surface hydrides at elevated temperatures (1250 and 1500 K). Furthermore, we observe that the iron carbide retains more surface hydride species, compared to the pure iron surface, at high temperatures, which is highly relevant for the activity of these catalysts in FT synthesis. We find that these retained hydride species predominantly cluster around the low-coordinated surface iron atoms on the iron carbide clusters. These results prove the ReaxFF capability of closing the gap between the QM description of small systems and short durations, and realistic large and complex systems undergoing longer simulation time, and its usefulness in evaluating new catalysts design processes.

In the future, we will expand our training set to include interactions with oxygen containing species. This will allow us to predict increasingly more complex reactions such as water formation and desorption, water gas shift reactions or catalysts poisoning, or to study the effect of material support upon catalytic properties. Progress in these areas is expected to create a strong foundation for simulations of FT synthesis processes.

Acknowledgments This work is funded by National Energy Technology Laboratory-Regional University Association (NETL-RUA). RES activity number 0004000.662.884.001.

References

1. Dry ME (2002) Catal Today 71:227–241
2. Davis BH (2003) Catal Today 84:83–98
3. Bozso F, Ertl G, Grunze M, Weiss M (1977) Appl Surf Sci 1:103–119
4. Burke ML, Madix RJ (1990) Surf Sci 237:20–34
5. Merrill PB, Madix RJ (1996) Surf Sci 347:249–264
6. Benziger J, Madix RJ (1980) Surf Sci 94:119–153
7. Benziger JB, Madix RJ (1982) Surf Sci 115:279–289
8. Blyholder G, Head J, Ruette F (1983) Surf Sci 131:403–418
9. Walch SP (1984) Surf Sci 143:188–203
10. Raeker TJ, DePristo AE (1990) Surf Sci 235:84–106
11. Jiang DE, Carter EA (2003) Surf Sci 547:85–98
12. Jiang DE, Carter EA (2004) Phys Rev B 70:64102–64110
13. Sorescu DC (2005) Catal Today 105:44–65
14. Mueller JE, van Duin ACT, Goddard WA III (2009) J Phys Chem C 113:20290–20306
15. Lo JMH, Ziegler T (2007) J Phys Chem C 111:11012–11025
16. Ono S, Mibeb K (2010) Phys Earth Planet Inter 180:1–6
17. Sorescu DC, Thompson DL, Hurley MM, Chabalowski CF (2002) Phys Rev B 66:035416–035428
18. Lo JMH, Ziegler T (2007) J Phys Chem C 111:13149–13162
19. Bromfield TC, Ferre DC, Niemantsverdriet JW (2005) Chemphyschem 6:254–260
20. Jiang DE, Carter EA (2003) Phys Rev B 67:214103–214113
21. Jiang DE, Carter EA (2004) Surf Sci 570:164–177
22. Sorescu DC (2008) J Phys Chem C 112:10472–10489
23. Sorescu DC (2006) Phys Rev B 73:15536–155420
24. Mayo SL, Olafson BD, Goddard WA III (1990) J Phys Chem 94:8897–8909
25. van Duin ACT, Dasgupta S, Lorant F, Goddard WA III (2001) J Phys Chem A 105:9396–9409
26. Raymand D, van Duin ACT, Baudin M, Hermansson K (2008) Surf Sci 602:1020–1031
27. Zhang Q, Cagin T, van Duin ACT, Goddard WA III, Qi Y, Hector LG (2004) Phys Rev B 69:045423–045433
28. Cheung S, Deng W-Q, van Duin ACT, Goddard WA III (2005) J Phys Chem A 109:851–859
29. Ojwang JGO, Santen RV, Kramer GJ, van Duin ACT, Goddard WA III (2008) J Chem Phys 128:164714–164722
30. Han SS, van Duin ACT, Goddard WA III, Lee HM (2005) J Phys Chem A 109:4575–4582
31. Goddard WA III, van Duin ACT, Chenoweth K, Cheng M-J, Pudar S, Oxgaard J, Merinov B, Jang YH, Persson P (2006) Top Catal 38:93–103
32. Ramasubramaniam A, Itakura M, Carter EA (2009) Phys Rev B 79:174101–174103
33. Mueller JE, van Duin ACT, Goddard WA III (2010) J Phys Chem C 114:4939–4949
34. Aryanpour M, van Duin ACT, Kubicki JD (2010) J Phys Chem A 114:6298–6307
35. Blochl PE (1994) Phys Rev B 50:17953–17979
36. Moroni EG, Kresse G, Hafner J (1997) Phys Rev B 56:15629–15646
37. Murnaghan FD (1944) Proc Natl Acad Sci 30:244–247
38. Henkelman G, Uberuaga BP, Jónsson H (2000) J Chem Phys 113:9901–9904
39. Sorescu DC (2009) J Phys Chem C 113:9256–9274
40. Mortier WJ, Ghosh SK, Shankar S (1986) J Am Chem Soc 108:4315–4320
41. Janssens GOA, Baekelandt BG, Toufar H, Mortier WJ, Schoonheydt RA (1995) J Phys Chem 99:3251–3258
42. van Duin ACT, Baas JMA, van de Graaf B (1994) J Chem Soc Faraday Trans 90:2881–2895
43. Acet M, Zahres H, Wassermann EF (1994) Phys Rev B 49:6012–6017
44. Blonski P, Kiejna A (2007) Surf Sci 601:123–133
45. Henriksson KOE, Sandberg N, Wallenius J (2008) Appl Phys Lett 93:191215–191912
46. Miyamoto G, Oh JC, Hono K, Furuhara T, Maki T (2007) Acta Mater 55:5027–5038
47. Tkacz M (2002) J Alloys Compd 330–332:25–28